Dynamic Strength of Adhesion Surfaces

Fang Li[1] and Deborah Leckband[2]

[1] Department of Theoretical and Applied Mechanics,

[2] Department of Chemical and Biomolecular Engineering,

University of Illinois at Urbana-Champaign

March 2, 2006

Abstract

We study theoretically the forced separation of two adhesive surfaces linked via a large number of parallel non-convalent bonds. We use a Brownian Dynamic simulation to compute the force-distance curve and the rupture force for separating adhesive surfaces with a constant rate. We also implement a statistical mechanics framework to describe the separating process, using a two-step reaction model with reaction rates obtained from the first passage time description for diffusive barrier crossing in a pulled-distance-dependent potential. A single integral mean first passage time (IMFPT) expression and the Kramers time are used to calculate the rate coefficients. The dependence of the rupture force on the separating rate exhibits three regimes. In the near-equilibrium regime, the rupture force asymptotically approaches the equilibrium rupture force, which is determined by the intrinsic free energy difference between two states. In the non-equilibrium regime, the rupture force increases with the separating rate and correlates with the bond rupture energy and the intrinsic off-rate. In the far from the equilibrium regime, the rupture force is determined by the bond rupture energy.

1 Introduction

Adhesive interactions between cells in multicellular organisms depend on specialized adhesion proteins found on cell surfaces. The molecular adhesion is based on short ranged nonconvalent specific interactions that are much stronger in comparsion with nonspecific forces [1]. Most adhesion molecules couple to the cytoskeleton and function under dynamic mechanical force in such essential processes as neuronal pathfinding, embryonic genesis, and white blood cell attachment to the wall of blood vessels. An understanding of molecular interactions under force is therefore important for models of signal transduction, cell motility, and other adhesion-controlled cellular functions.

Over the past decade, single molecule force measurement techniques, such as atomic force microscopy and optical tweezers, have been extensively used to explore the dissociation of

nonconvalent bonds. In such experiments, the force probe is attached by a flexible linker to a molecule, moved into a position where the molecule can bind to a corresponding molecule on a fixed surface, and then pulled away at a constant velocity. The external force needed to break the bond under a given loading rate is measured, the magnitude of the force exhibits a distribution rather than a determined value [2, 3, 4]. To explain the distribution of the rupture forces, the dissociation of a bond is modelled as the thermally assisted crossing of an activation barrier in the framework of the Kramers diffusion theory of chemical reactions [5]. The external force modifies the molecular interaction potential that determines the chemical kinetics. By assuming that the force linearly diminishes the activation energy barrier, one finds that the rate coefficient depends on the time dependent external force by the relation [6, 7]

$$k_{\rm off}(t) = k_0 \exp[f(t)\Delta x]\,. \tag{1}$$

Eq. 1 is most commonly used to analyze the pulling experiments due to the explicit description of the coupling between the off-rate and the force. This formula is also an extension of Bell's model that was first proposed [8] to describe the off-rate under a constant force. However, the assumption that the force changes the energy barrier linearly limits the range of the validity [9] to the diffusive barrier crossing under small forces. Hummer [10] used the Kramer time to calculate the off-rate for a harmonic potential with a sharp barrier. A simple expression of off-rate valid for a high barrier was derived. Based on the predicted average rupture force under linear loading, they developed an alternative way to extract the intrinsic off-rate from single bond rupture experiments.

The above descriptions apply to single molecular bonds. In biological systems, the number of ligand–receptor pairs mediating adhesive contacts between cells varies from a few (for tethering leukocytes to vessel walls) to $> 10^5$ (mature cell–matrix contact). While characterizing adhesive bonds at the single molecule level provides insights into the physics of nonconvalent bond rupture under a dynamic force, it is more biologically relevant to understand what determines the strength of adhesion mediated by multiple bonds in parallel. One of the main differences between the two systems is that multiple bond contact allows for rebinding [11, 12], which rarely happens for single bond rupture under force [13]. The reason is that for a single bond, the bond is pulled apart by the elastic relaxation of a linker molecule and there is no constraint to keep the ruptured pair close enough to rebind. Ruptured bonds between two extended surfaces, however, can rebind as long as the distance between the surfaces is held close by the survived bonds.

For adhesion involving a small number of bonds, the number of survived bonds in the adhesive contact is a time-dependent random variable that fluctuates significantly. The stochastic kinetics can be described by a master equation using the probability theory for kinetics of a small system [14]. The master equation has been solved numerically for adhesion mediated by no more than ten bonds, for the scenarios involving a constant force [15, 16] or a linear loading [17]. A mathematically equivalent approach is to use Monte Carlo simulation. Each bond in the system can be switched between two states (on and off) at different time steps. In this manner, the chemical kinetics can be coupled to more complicated processes. For example, the adhesive dynamics method combines the analysis of particle motion in flow

with a Monte Carlo simulation of chemical kinetics describing the survival and rupture of the ligand-receptor bonds. The simulation predicts a phase diagram [18] of different particle motions based on values of the intrinsic on-rate k_f^0 and the fitting parameter Δx in Eq. 1. The simulation results can be directly compared to flow chamber experiments where ligand-coated beads are driven by a flow with controllable velocity over a surface bearing receptors.

For adhesive contacts with a large ensemble of bonds, the most important quantity to describe the adhesion between surfaces is the average number of survived bonds. The geometry of the model is generically set as shown in Fig. 1. A phenomenological description based on a rate equation can be used to describe the evolution of the survived population under external forces [8, 19]. Obviously, the choice of the reaction constants used in the rate equation directly determine the survived population during a pulling process. The present understanding relating the calculation of rate coefficients for thermally activated barrier crossing has been surveyed in a review paper by Hänggi et al. [20].

Bell [8] analyzed the kinetics of reversible bonds under a constant force, and calculated the equilibrium strength of surface adhesion, using Bell's model for the off-rate and assume that the on-rate is unaffected by the applied force. Seifert [19] used the same dependence of the kinetic rates on an imposed dynamic force and implemented a scaling analysis of the rate equation to reveal different loading regimes for the rupture force. But the results are erroneous due to an incorrect scaling of the rate equations. Seifert [12] constructed a rather elaborate statistical mechanics framework to estimate the bulk force required to rupture two adherent surfaces when the surfaces are separated with a constant separating rate v. However, using one-step reaction model with rates calculated from the Kramers rate formula [5], he assumed both the rupture barrier and the rebindng barrier satisfy U>> $k_{\mathrm{B}}T$. The assumption does not hold for the separating process of two surfaces linked by nonconvalent bonds. The rupture barrier for a nonconvalent adhesion bond is of order 1-20 $k_{\mathrm{B}}T$, as shown in various of measurements [21, 22]. The intrinsic rebinding barrier is smaller than the rupture barrier. It is also likely that the height of the rupture barrier becomes comparable with $k_{\mathrm{B}}T$ as the force applied changes energy profile during a pulling process. The Kramers rate formulae (both for the smooth barrier and for the edge-shaped barrier) hold only if the energy barrier U is much greater than $k_{\mathrm{B}}T$ [20]. Thus, the Kramers rate formula can not accurately predict the rate constants for bonds rupture and formation during a pulling process.

In this paper, we addressed some remaining questions based on previous work. First of all, how to apply Seifert's statistical mechanics framework for the process of separating parallel non-convalent bonds? Second, why does the dependence of the rupture force on loading rates vary in different puling rate regimes? How to estimate loading rates that define the crossover between different regimes? Finally, How does the rupture force correlate with the thermodynamic and kinetic parameters in different regimes?

We use a Brownian dynamics simulation to compute the force-distance curve and the rupture force for separating adhesive surfaces with a constant rate. The model assumes a superposition of the intrinsic ligand-receptor force, the shared external pulling force, and the Brownian force along the pulling coordinate. The relative position of an adhesion pair along

the pulling coordinate, which is correlated to the state of the bond, is determined by the over-damped Langevin equation. This allows to determine the state of each bond and the total force exerted on the surface as a function of pulled distance.

We also use a two-step reaction model to describe the kinetics and implement rate coefficients based on a single integral mean first passage time (IMFPT) [23] and the Kramers time for a sufficiently high barrier. In Section 3.1, we compare the rate constants in a pulling process based on the IMFPT expression with those based on the Kramers time. We show the evolution of the survived bond population in a pulling process calculated from the two-step rate equation using the IMFPT expression agrees with that obtained from Brownian dynamics simulations. Using the Brownian dynamics simulations, We also verify the assumption that the survived bonds are Boltzmann-distributed in the on-state. Finally, we show that the rupture forces calculated from the statistical mechanics framework with reaction rates using the IMFPT expression match those obtained from Brownian dynamics simulations.

Finally, we show that the dependence of the rupture forces and the separating rate falls into three regimes: near-equilibrium, non-equilibrium and far-from-equilibrium. In the near-equilibrium regime, the separating rate v is slower than a critical rate. In this regime, the rupture force asymptotically approaches the equilibrium rupture force, which is determined by the intrinsic free energy difference between two states. In Section 3.3, we derive the expression for estimating the critical separating rate using a simple physical argument. The value of the predicted critical separating rates for various systems are in good agreement with the results from Brownian Dynamic simulations. In In Section 3.4, we show that in the non-equilibrium regime, the rupture force increases with the separating rate and correlates with the bond rupture energy and the intrinsic off-rate. In the far from the equilibrium regime where the rebinding is relevent, the rupture force is determined by the bond rupture energy.

2 Theory

2.1 A model for molecular adhesion between surfaces

Suppose two surfaces, joined by adhesive molecules as shown in Fig. 1(A), are pulled apart at a constant rate v, separate a distance $L = vt$ after time t. We will consider the motion of two molecules along the pulling coordinate, measuring the distance between the paired adhesion molecules along this coordinate by the variable x. In this case, we assume that the total potential

$$U(x, L) = U_0(x) + U_s(x, L)\,, \tag{2}$$

where $U_0(x)$ is the intrinsic energy for an adhesion pair. An example of a typical potential at a pulled distance L is shown in Fig. 1B. $U_s(x, L)$ is due to the external force transmitted at the separation distance L by the linker that connects the molecule to the surface in Fig. 1(A). Theoretically, one can obtain the bond rupture energy profile from the single molecule pulling experiments [24, 25]. The instantaneous energy along the pulling path can also be computed

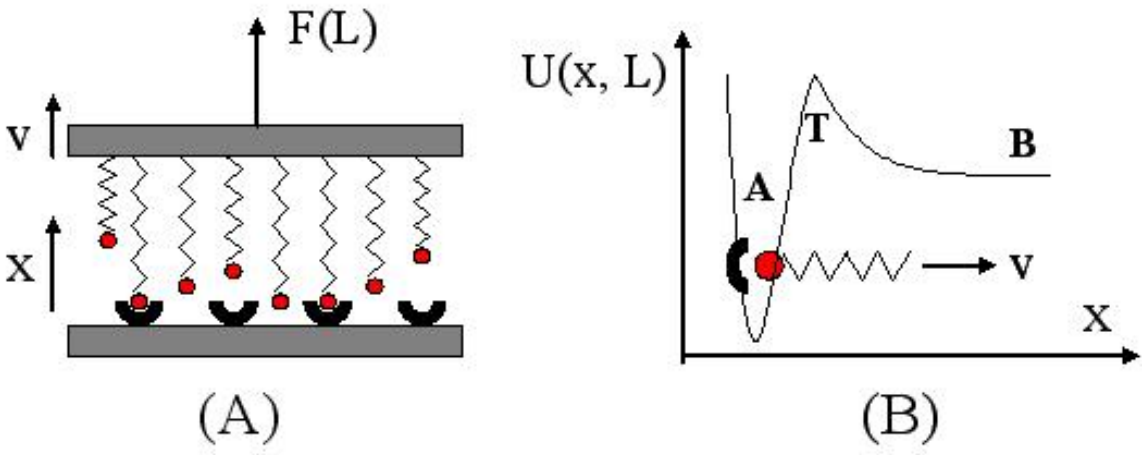

Figure 1: (A) shows a schemetic view of our model. The top surface bears molecules tethered by identical soft linkers and N_0 complementary molecules are confined to a parallel fixed surface on the bottom. The top surface is moving with a constant rate v normal to the surface. For a given pair of molecules, the coordinate x measures the distance between the paired adhesion molecules along the pulling direction. The pulled distance since the initial time is $L = vt$. The total force applied $F(L)$ is measured as a function of the pulled distance L. (B) shows a typical bond potential $U_0(x)$, as a function of the reaction coordinate x. The adhesion bonds can be in the bound state A, the transition state T, and the free state B.

from Molecular dynamics simulations [7]. In this work, we choose $U_0(x)$ to be

$$U_0(x) = \frac{1}{2}k_{\rm A}(k_{\rm A} - x)^2 \ \text{ for } x \le x_{\rm T}, \tag{3}$$

$$U_0(x) = \frac{1}{2}k_{\rm B}(x_{\rm B} - x)^2 + \Delta U_0 \ \text{ for } x_{\rm T} < x < x_{\rm B}. \tag{4}$$

$$U_0(x) = \Delta U_0 \ \text{ for } x > x_{\rm B}. \tag{5}$$

Here $k_{\rm A}$ and $k_{\rm B}$ are the curvatures of the energy profile in state A and B. $x_{\rm A}$ and $x_{\rm B}$ are the equilibrium positions of states A and B. $x_{\rm T}$ is the position of the transition state. ΔU_0 is the energy difference of the two energy minima. We assume the pulling force is harmonic

$$U_s(x, L) = \frac{1}{2}k(L - x)^2\,, \tag{6}$$

where k is the spring constant, L is the pulled distance $L = vt$ at time t with a constant separating rate v.

2.2 A Brownian dynamics simulation describing the pulling process

We use Kramers's one dimensional diffusion model to describe the rupture of a nonconvalent bond between an adhesion molecule pair. The molecules undergo Brownian motion in a

force field. The distance x between a pair of adhesion molecules evolves according to the over-damped Langevin equation,

$$\gamma\dot{x} = -\partial_x U(x,t) + \xi(t) \ , \ \langle \xi(t) \rangle = 0 \ , \ \langle \xi(0)\xi(t) \rangle = 2\gamma k_B T \delta(\Delta t) \, . \tag{7}$$

Here, γ is the drag coefficient, $-\partial_x U(x,t)$ is the systematic force between the paired adhesion molecules, and $\xi(t)$ is a Brownian random force with mean zero force and variance $2\gamma k_B T$.

A second order Runge-kutta method gives a more accurate and stable integrator. Rewriting the Langevin equation as a finite difference equation:

$$x_1 = x(t) + \Delta t(-\partial_x U(x,t)) + \sqrt{2D\Delta t} R(t) \, , \tag{8}$$

$$x_2 = x(t) + \Delta t(-\partial_x U(x_1,t)) + \sqrt{2D\Delta t} R(t) \, , \tag{9}$$

$$x(t+\Delta t) = x_1 + x_2. \tag{10}$$

where diffision coefficient $D = k_B T/\gamma$, and $R(t)$ is a Gaussian random number of unit variance. A system of N_0 pairs correspond to N_0 trajectories.

In this model, we assume that different bound pairs do not interact with each other. Therefore, Eq. 7 can be solved individually for different bonds. We implemented a computer program to solve the stochastic differential equation. The Gaussian random number $R(t)$ is generated by applying the Box-Muller transformation [26] to the uniform distributed random numbers given by the `ran2` [27] subroutine. In the program, we can vary the parameters of the intrinsic energy profile k_A, k_B, x_A and x_B, the stiffness of the pulling linker k, and the separating rate v. To model the system includes N_0 bonds, we generate N_0 independent trajectories. Using the trajectories, we then calculate the important features of the system that we are interested in. For example, the population of the survived bonds $N_{\rm A}(L)$, the distribution of the survived population in the bound state, and the external force $F(L)$ measured when the two surfaces are separated with a constant separating rate v can be easily computed from the trajectories. For a typical simulation with $N_0 = 10,000$ and $\Delta t = 0.001$ ns, the computer program required about an hour of execution time on a Pentium 4 PC to run a 1 μs simulation.

2.3 Rate equation for the kinetics of rupture

The phenomenlogical description based on a rate equation has long been used for describing the average behavior of adhesive bonds [8, 12, 10]. We use a 3-state model and denote the three states as the bound state A, the transition state T, and the free state B as shown in Fig. 1(B). We consider the transition between the state A and the state B as a two-step reaction $A \rightleftharpoons T \rightleftharpoons B$.

Since the bonds in state T will relax quickly to A or B, we assume that T is always at steady-state with its infinitesimal population, and we can use a first order kinetic equation to describe the reaction. Let $k_{\rm off}(L)$ be the off-rate from state A to state B, and $k_{\rm on}(L)$ the on-rate from B to A. For a large ensemble of bonds, the fluctuation between state A and B is less important. and the population in state A and B approximate to the average number.

Thus, we have a rate equation to describe how the population in state A changes with the pulled distance L under a constant separating rate v:

$$v\frac{dN_{\rm A}(L)}{dL} = -k_{\rm off}(L)N_{\rm A}(L) + k_{\rm on}(L)(N_0 - N_{\rm A}(L))\,. \tag{11}$$

In order to proceed with our calculation, we need values for the kinetic rates. These come directly from the potential $U(x, L)$, according to the formula of rate constants from either the Kramers rate formula or the IMFPT expression. Both of the formulae are originally defined for a time independent thermodynamic system, but are used to determine the rates of transition between nonequilibrium states for driven Brownian motion in a time-dependent potential [20]. Notice the kinetic rates $k_{\rm on}(L)$ and $k_{\rm off}(L)$ are functions of the pulled distance L. The reason is that the pulling force changes the potential $U(x, L)$, including the equilibrium positions $x_{\rm A}$ and $x_{\rm B}$. The instantaneous kinetic rates at a pulled distance L are

$$k_{\rm off}(L)^{-1} = \tau(p^{\rm A}_{eq}(x, L), x_{\rm T}) + \tau(p^{\rm B}_{eq}(x, L), x_{\rm T})Z_{\rm A}/Z_{\rm B}\,, \text{ and} \tag{12}$$

$$k_{\rm on}(L)^{-1} = \tau(p^{\rm B}_{eq}(x, L), x_{\rm T}) + \tau(p^{\rm A}_{eq}(x, L), x_{\rm T})Z_{\rm B}/Z_{\rm A}\,. \tag{13}$$

$k_{\rm on}(L)/k_{\rm off}(L) = Z_{\rm A}/Z_{\rm B}$ is used to derive Eq. 12, 13. $Z_{\rm A}$ and $Z_{\rm B}$ represent the partition functions which are defined as

$$Z_{\rm A} = \int_0^{x_{\rm T}} dx \exp[-U(x)/k_{\rm B}T]\,, \text{ and} \tag{14}$$

$$Z_{\rm B} = \int_{x_{\rm T}}^{\infty} dx \exp[-U(x)/k_{\rm B}T]\,. \tag{15}$$

The IMFPT $\tau(1, 2)$ is defined as the average time elapsed for a bond to start at state 1 and reach state 2 at the first time. $\tau(p^{\rm A}_{eq}(x, L), x_{\rm T})$ and $\tau(p^{\rm B}_{eq}(x, L), x_{\rm T})$ represent the IMFPT for an equilibrium distribution of bonds in state A and B to transition position $x_{\rm T}$, respectively,

$$\tau(p^{\rm A}_{eq}(x, L), x_{\rm T}) = \int_0^{x_{\rm T}} dx [D p^{\rm A}_{eq}(x, L)]^{-1} \int_0^{x} dy p^{\rm A}_{eq}(y, L)\,, \text{ and} \tag{16}$$

$$\tau(p^{\rm B}_{eq}(x, L), x_{\rm T}) = \int_{x_{\rm T}}^{\infty} dx [D p^{\rm B}_{eq}(x, L)]^{-1} \int_{x}^{\infty} dy p^{\rm B}_{eq}(y, L)\,, \tag{17}$$

where the equilibrium distribution $p^{\rm A}_{eq}(x, L)$ and $p^{\rm B}_{eq}(x, L)$ are defined as

$$p^{\rm A}_{eq}(x, L) = Z^{-1}_{\rm A}(L) \exp[-U(x)/k_{\rm B}T]\,, \text{ and} \tag{18}$$

$$p^{\rm B}_{eq}(x, L) = Z^{-1}_{\rm B}(L) \exp[-U(x)/k_{\rm B}T]\,. \tag{19}$$

The formula for the calculation of the IMFPT is directly generated from the exact solution of the one dimensional Smoluchowski equation. The reaction dynamics it predicts are in a good agreement with the exact numerical calculation including the limit when the energy

barrier is comparable to $k_{\mathrm{B}}T$ [23]. For a potential profile with a high edge-shaped barrier $U >> k_{\mathrm{B}}T$, the IMFPT can be simplified to a formula similiar to the Kramers time,

$$\tau(x_{\mathrm{A}}(L), x_{\mathrm{T}}) = \frac{\gamma}{k_{\mathrm{A}} + k}\sqrt{\pi\frac{k_{\mathrm{B}}T}{U_1(L)}}\exp[\frac{U_1(L)}{k_{\mathrm{B}}T}]\,, \text{ and} \tag{20}$$

$$\tau(x_{\mathrm{B}}(L), x_{\mathrm{T}}) = \frac{\gamma}{k_{\mathrm{B}} + k}\sqrt{\pi\frac{k_{\mathrm{B}}T}{U_2(L)}}\exp[\frac{U_2(L)}{k_{\mathrm{B}}T}]\,. \tag{21}$$

Here $U_1(L)$ and $U_2(L)$ are the height of the rupture barrier and the rebinding barrier at the pulled distance L.

2.4 Measuring the rupture force in phenomenlogical description

At the equilibrium separation under zero separating rate, we assume the distribution of bonds on the energy profile satisfies the Boltzmann distribution,

$$N_{\mathrm{A}}^{eq} = N_0 * \int_0^{x_{\mathrm{T}}} dx[-U(x, L)] / \int_0^{\infty} dx[-U(x, L)]\,. \tag{22}$$

The force measured at the pulled distance L is given by

$$F(L) = N_0 * \int_0^{\infty} dx\, k(L - x)\exp[-U(x, L)] / \int_0^{\infty} dx\exp[-U(x, L)]\,. \tag{23}$$

We define the peak of the force distance curve as the equilibrium rupture force F_{eq}^r, and define the corresponding pulled distance as the equilibrium rupture distance L_{eq}^r. Given the knowledge of the individual bond energy profile, Eq. 23 can be used to estimate the equilibrium rupture force of adhesive surfaces.

If thermal equilibrium between the two states is not satisfied for a pulling process with a separating rate, the above method is not applicable. We assume the intrinsic molecular interaction is short-ranged and the survived bonds are the main contribution to the measured force. We also assume the survived bonds in state A satisfy the Boltzmann distribution during a pulling process. Thus, the total force exerted by the bonds can be calculated, based on the survived population in each potential well described by the rate Eq. 11. The total force can then be expressed as

$$F(L) = N_{\mathrm{A}}(L) * f(L)\,, \tag{24}$$

$$f(L) = \int_0^{x_{\mathrm{T}}} dx\, k(L - x)\exp[-U(x, L)] / \int_0^{x_{\mathrm{T}}} dx\exp[-U(x, L)]\,. \tag{25}$$

3 Results and Discussion

3.1 Comparison of kinetic rate models

In Section 2 , we described two different methods to estimate the chemical kinetic rate constants. Fig. 2 shows the estimated rate constants using the kramers time formula deviate

from those using the IMFPT expression in a pulling process when the energy barriers do not satisfy $U >> k_{\rm B}T$. As a further illustration of the comparsion, Fig. 3 shows the evolution of the survived bond population in a pulling process calculated from the rate equation using the IMPFT expression matches with that from the Brownian dynamics simulations for different separating rates, In addition, Fig. 4, the instanetuous distribution of the survived population obtained from the Brownian dynamics simulations, shows a Boltzmann distribution in the bound state. Thus, we can expect the rupture force calculated from Eq. 24 using the IMPFT expression agree with that from the Brownian dynamics simulations, as shown in Fig. 7.

3.2 Kinetically trapped in the bound state cause excess force

As shown in Fig. 5, $N_{\rm A}(L)$ approaches the value for the equilibrium separation predicted from Eq. 22 At slow separating rates. For a pulled distance L, the faster the separating rate, the larger is $N_{\rm A}(L)$. The reason is that with the faster separating rate, the bonds are given less time to escape to the free state for a certain surface pulled distance. The observation that more bonds are kinetically trapped in the bound state with faster pulling is also shown in force curves in Fig. 6. In the first stage of the surface separation, the force curves for different separating rates overlap and increase linearly with the pulled distance with the slope as the pulling spring constant $k = 1.0$. The reason is that most of the bonds are in the bound state, and the force increases linearly due to the elongation of the linkers. In the second stage, the bonds start to escape to the free state. The force curves for different separating rates separate and reach the maximum at different distances. For the same pulled distance, the force achieved at faster separating rates are larger since more bonds are trapped in the bound state, which are the main contribution to the total force. In the third stage, all the bonds ruptured and the calculated force is the hydrodynamic force and increases linearly with the separating rate.

3.3 Near-equilibrium rupture

As shown in the Fig. 8, the rupture force asymptotically approaches the equilibrium rupture force F^r_{eq} normalized by the total bonds at the initial time N_0, 2.5916. 2.5895, 3.1168, 3.3566 for the four molecular pairs. The rupture force reaches F^r_{eq} if the separating rate is slower than a critical separating rate, which can be derived using a simple physical argument. If the separating distance reaches L^r_{eq} slow enough so that the system is given enough time to relax to the thermal equilibrium on the energy potential corresponds to the equilibrium rupture distance L^r_{eq}, the rupture force approaches the equilibrium value.

We know that a system initially in state A relaxes exponentially,

$$N_{\rm A}(t) = C_1 + C_2 \exp[-((k_{off}(L^r_{eq}) + (k_{on}(L^r_{eq}))t] \tag{26}$$

with $C_1 = -C_2 = Z_A(L^r_{eq})/(Z_A(L^r_{eq}) + Z_B(L^r_{eq}))$, and the relaxation time is defined as

$$\tau = (k_{off}(L^r_{eq}) + k_{on}(L^r_{eq}))^{-1} \tag{27}$$

On one hand, it takes the system time $t >> \tau$ for the number of the bonds between state A and state B to equilibrate on the potential corresponding to the moved distance L^r_{eq}. On the other hand, the time that it takes for moving surface the distance L^r_{eq} is give by L^r_{eq}/v. A separating rate that gives the system a time longer than the relaxation time can ensure that the system will rupture near equilibrium. Thus the critical separating rate v_c satisfies

$$v_c >> L^r_{eq}/\tau \tag{28}$$

Example values of L^r_{eq}/τ are shown in Table 1. By comparing the values of the critical separating rate to the locations of the asymptotes plotted in Fig. 8, we see that the estimation from Eq. 28 is in a good agreement with the results from Brownian dynamics simulations.

As shown in the Fig. 9, the rupture force in the near-equilibrium regime is not correlated with both the intrinsic kinetic rates and the rupture energy barrier, but the free energy difference, $Ln(k_{\text{on}}/k_{\text{off}})$.

3.4 Non-equilibrium rupture

If the separating rate is above the critical separating rate v_c, the excess of the rupture force over the equilibrium rupture force F^r_{eq}. As shown in the Fig. 9, the rupture force in the non-equilibrium regime is correlated with both the the logarithm of intrinsic off-rate and the rupture energy barrier instead of the the free energy difference.

In the far-from-equilibrium regime, the rebinding is not important. Theoretical prediction of this regime has been given by Hummer [10]. Fig. 9 shows a clear correlation of the rupture force with the logarithm of intrinsic off-rate and the rupture energy barrier.

4 Future work

We have shown that Brownian dynamics simulation is accurate and straightforward in describing the kinetics of molecules which determine adhesive interactions between two separating surfaces. We look for the correlation between the rupture force and the measurable thermodynamic parameters in different loading regimes. We can compare our predictions with experiments and physiological processes. Furthermore, Brownian dynamic simulation is easily implemented to simulate rupture under a variety of physical conditions in order to compare with experiments. For example, we can add the curvature of the two surfaces in the model in order to compare the surface force measurements.

References

[1] D. E. Leckband, F. J. Schmitt, J. N. Israelachvili, and W. Knoll. Direct force measurement of specific and nonspecific protein interactions. *Biochem.*, 33:4611–4624, 1994.

[2] E. L. Florin, V. T. Moy, and H. E. Gaub. Adhesive forces between individual ligand-receptor pairs. *Science*, 264:415–417, 1994.

[3] R. Merkel, P. Nassoy, A. Leung, K. Ritchie, and E. Evans. Energy landscapes of receptor-ligand bonds explored with dynamic force spectroscopy. *Science*, 397:50–53, 1999.

[4] M. Benoit, D. Gabriel, G. Gerisch, and H. E. Gaub. Discrete interactions in cell adhesion measured by single-molecule force spectroscopy. *Nat. Cell Biol.*, 2:313–317, 2000.

[5] H. A. Kramers. Brownian motion in a field of force and the diffusion model of chemical reactions. *Physica.*, 7:284–304, 1940.

[6] E. Evans and K. Ritchie. Dynamic strength of molecular adhesion bonds. *Biophys. J.*, 72:1541–1555, 1997.

[7] S. Izrailev, S. Stepaniants, M. Balsera, Y. Oono, and K. Schulten. Molecular dynamics study of unbinding of the avidin-biotin complex. *Biophys. J.*, 72:1568–1581, 1997.

[8] G. I. Bell. Models for the specific adhesion of cells to cells. *CScience*, 200:618–627, 1978.

[9] M. Dembo, D. C. Torney, K. Saxman, and D. Hammer. The reaction-limited kinetics of membrane-to-surface adhesion and detachment. *Proc. R. Soc. Lond. B Biol. Sci.*, 234:55–83, 1988.

[10] G. Hummer and A. Szabo. Kinetics of nonequilibrium single-molecule pulling experiements. *Biophys. J.*, 85:5–15, 2003.

[11] R. Vijayendran, D. Hammer, and D. Leckband. Simulation of the adhesion between molecularly bonded surfaces in direct force measurements. *J. of Chem. Phys.*, 108:7783–7794, 1998.

[12] U. Seifert. Dynamic strength of adhesion molecules: Role of rebinding and self-consistent rates. *Europhys. Lett.*, 58(5):792–798, 2001.

[13] E. Evans. Probing the relation between force - lifetime - and chemistry in single molecular bonds. *Annu. Rev. Biophys. Biomol. Struct.*, 30:105–128, 2001.

[14] McQuarrie D. A. Kinetics of small systems. *J. of Chemistry and Physics*, 38:433–436, 1963.

[15] G. Kaplanski, C. Farnarier, O. Tissot, A. Pierres, A. M. Benoliel, M. C. Alessi, S. Kaplanski, and P. Bongrad. Granulocyte-endothelium initial adhesion. analysis of transient binding events mediated by e-selectin in a laminar shear flow. *Biophys. J*, 64:1922–1933, 1993.

[16] T. Erdmann and U. S. Schwarz. Stability of adhesion clusters under constant force. *Phys. Rev. Lett.*, 92(10):108102 1–4, 2004.

[17] T. Erdmann and U. S. Schwarz. Adhesion clusters under shared linear loading: A stochastic analysis. *Europhys. Lett.*, 66(4):603–609, 2004.

[18] K. C. Chang, D. F. Tees, and D. A. Hammer. The state diagram for cell adhesion under flow: leukovyte rolling and firm adehsion. *Proc. Natl. Acad. Sci.*, 97:11262–11267, 2000.

[19] U. Seifert. Rupture of multiple parallel molecular bonds under dynamic loading. *Phys. Rev. Lett.*, 84(12):2750–2754, 2000.

[20] P. *Hänggi*, P. Talker, and M. Borkovec. Reaction-rate theory: fifty years after kramers. *Rev. of Modern Phys.*, 62(2):252–341, 1990.

[21] B. Zhu, S. C. Flament, E. Wong, I. E. Jensen, B. M. Gumbiner, and D. Leckband. Functional analysis of the structural basis of homophilic cadherin adhesion. *Biophys. J.*, 84:4033–4042, 2003.

[22] E. Perret, A. Leung, H. Feracci, and E. Evans. Trans-bonded pairs of e-cadherin exhibit a remarkable hierarchy of mechanical strengths. *Proc. Natl. Acad. Sci*, 101(47):16472–16477, 2004.

[23] K. Schulten, Z. Schulten, and A. Szabo. Dynamic strength of adhesion molecules: Role of rebinding and self-consistent rates. *Europhys. Lett.*, 74(8):4426–4432, 1981.

[24] C. Jarzynski. Nonequilibrium equality for free energy differences. *Phys. Rev. Lett.*, 78:2690–2693, 1997.

[25] G. Hummer and A. Szabo. Free enery reconstruction from nonequilibrium single-molecule pulling experiment. *Proc. Natl. Acad. Sci.*, 98:3658–3661, 2001.

[26] G. E. Box and M. E. Muller. A note on the generation of random normal deviates. *Ann. Math. Stat.*, 29:610–611, 1958.

[27] W. H. Press, B. P. Flannery, A. Teukolsky, and W. T. Vetterling. *Numerical Recipes in Fortran*. Cambridge University Press, New York, NY, 1992.

Pair	F^r_{eq}/N_0	L^r_{eq}	τ	L^r_{eq}/τ
A	2.5916	2.05	82.6	0.0056
B	2.5895	2.02	361	0.0107
C	3.1168	2.53	237	0.0015
D	3.3566	2.73	2020	0.0010

Table 1: Estimate the critical separating rates for the four molecular pairs in Fig. 8. The equilibrium rupture force f^r_{eq} is the peak in the force-distance curve described by Eq. 23. The equilibrium rupture distance L^r_{eq} is the pulled distance corresponding to the peak in the force-distance curve. The relaxation time τ is calculated from Eq. 27. The critical separating rate L^r_{eq}/τ is calculated according to Eq. 28.

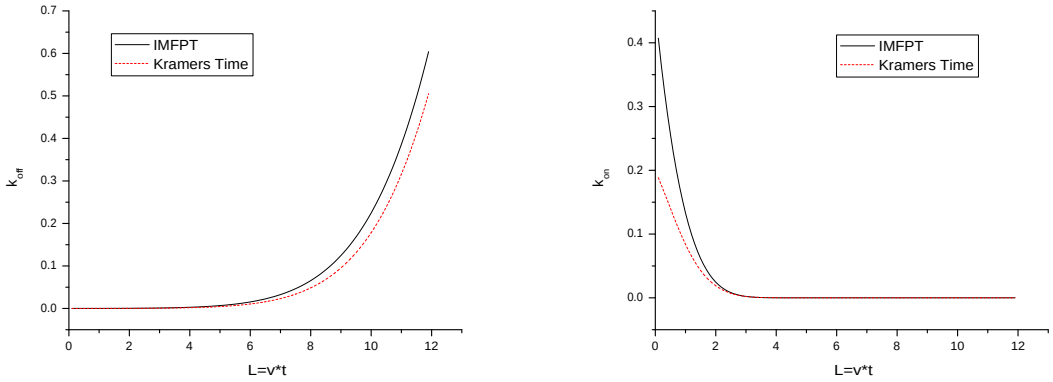

Figure 2: Rates constants, $k_{\rm off}(L)$ and $k_{\rm on}(L)$, as a function of the pulled distance L. The solid curve uses the IMFPT expressions in Eq. 16 and Eq. 17. The dashed curve uses the Kramers time formulae in Eq. 20 and Eq. 21. The parameters used are $U_1 = 12$, $k_1 = 24$, $U_2 = 2$, $k_2 = 1$, $k = 1$, $\gamma = 1$. The units used in the computation are $k_{\rm B}T$ for the energy, $4.1pN$ for the force, nm for the distance, and ns for the time.

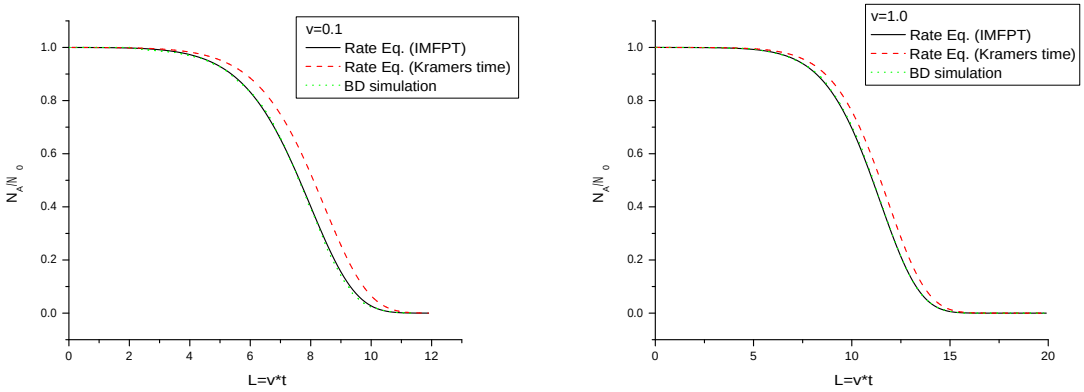

Figure 3: Survived population $N_{\rm A}(L)$, normalized by the total bonds at the initial time N_0, as a function of the pulled distance L for $v = 0.1$ and $v = 1.0$. $N_{\rm A}(L)$ is calculated by three methods. The solid curve is from the rate equation Eq. 11 with rates using the IMFPT expressions in Eq. 16 and Eq. 17. The solid curve is from the rate equation with rates using the Kramers time in Eq. 20 and Eq. 21. The dotted curve is obtained from the Brownian dynamics simulations. Other parameters are the same as in Fig. 2.

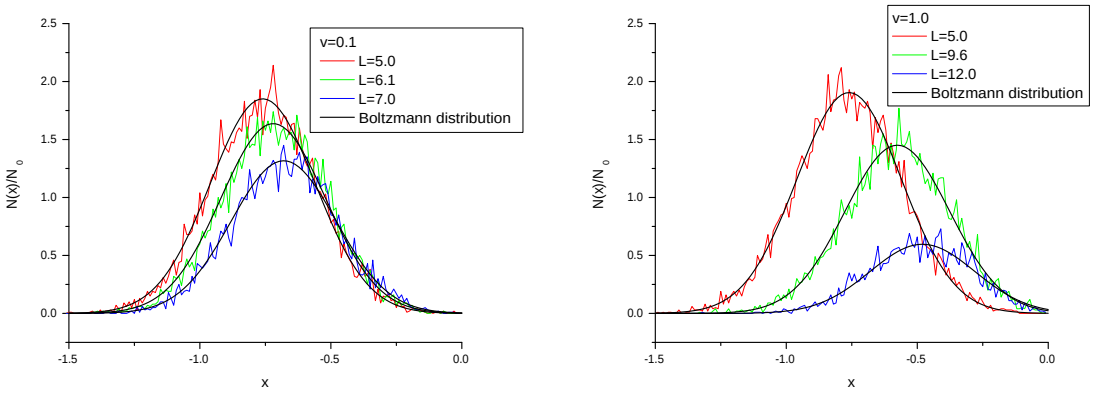

Figure 4: Distribution of the normalized survived population for $v = 0.1$ and $v = 1.0$ obtained from Brownian dynamics simulations. Three curves correspond to three pulled distance, before-rupture-distance, at-rupture-distance, and after-rupture-distance. The fitting lines are calculated assuming the distribution of the survived bond population satisfy Boltzmann distribution. Other parameters are the same as in Fig. 2.

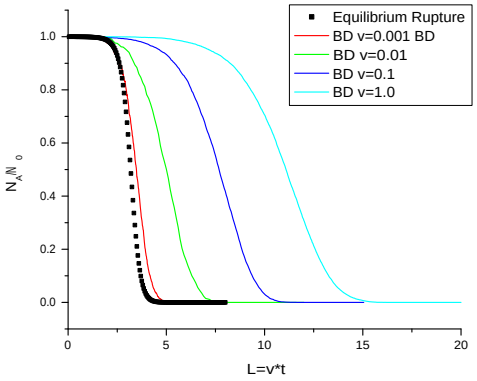

Figure 5: The normalized survived population $N_{\rm A}(L)/N_0$ as a function of the pulled distance L for various separating rates. The survived bond population $N_{\rm A}(L)$ is obtained from the Brownian dynamics simulations. The separating rates are, from left to right, $v = 0.001$, 0.01, 0.1, 1.0. The squares are obtained from Eq. 22 for $v = 0$. Other parameters are the same as in Fig. 2.

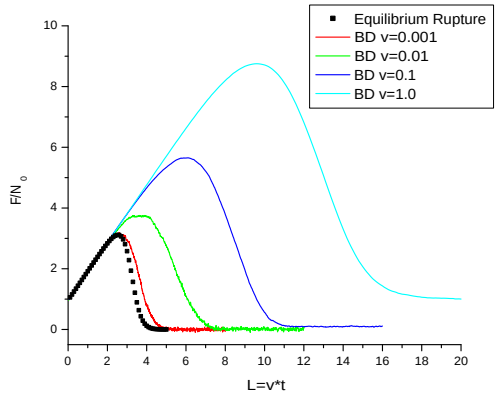

Figure 6: The normalized rupture force $F(L)/N_0$ as a function of the pulled distance L for various separating rates. The total force $F(L)$ is obtained from the Brownian dynamics simulations. The separating rates are, from left to right, $v = 0.001$, 0.01, 0.1, 1.0. The squares are obtained from Eq. 22 for $v = 0$. Other parameters are the same as in Fig. 2.

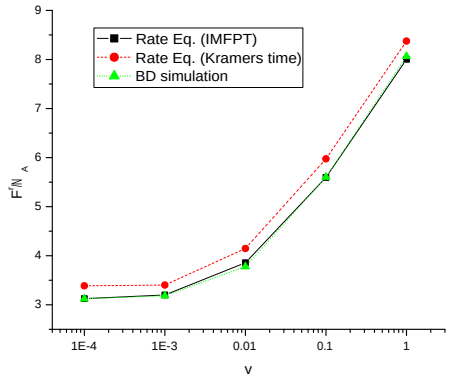

Figure 7: The normalized rupture force F^r/N_0 as a function of the separating rate v. The total force F^r is calculated from three methods: Eq. 24 with rates using the IMFPT expressions, Eq. 24 with rates using the Kramers time formulae, and the Brownian dynamics simulations. The rupture force is assumed as the peak of the force-distance curve. Other parameters are the same as in Fig. 2.

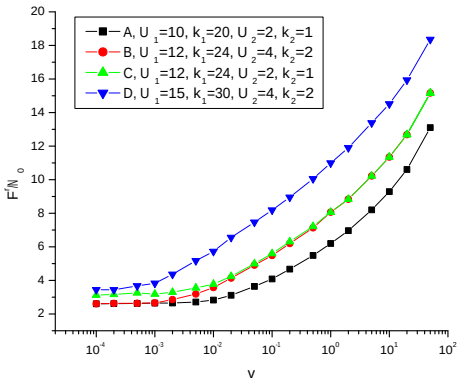

Figure 8: The normalized rupture force F^r/N_0 as a function of the separating rate v. The total force F^r is calculated from the Brownian dynamics simulations. The rupture force is assumed as the peak of the force-distance curve in Fig. 6. The rupture force is computed for various molecular parameters as shown in the plot. Other parameters are the same as in Fig. 2.

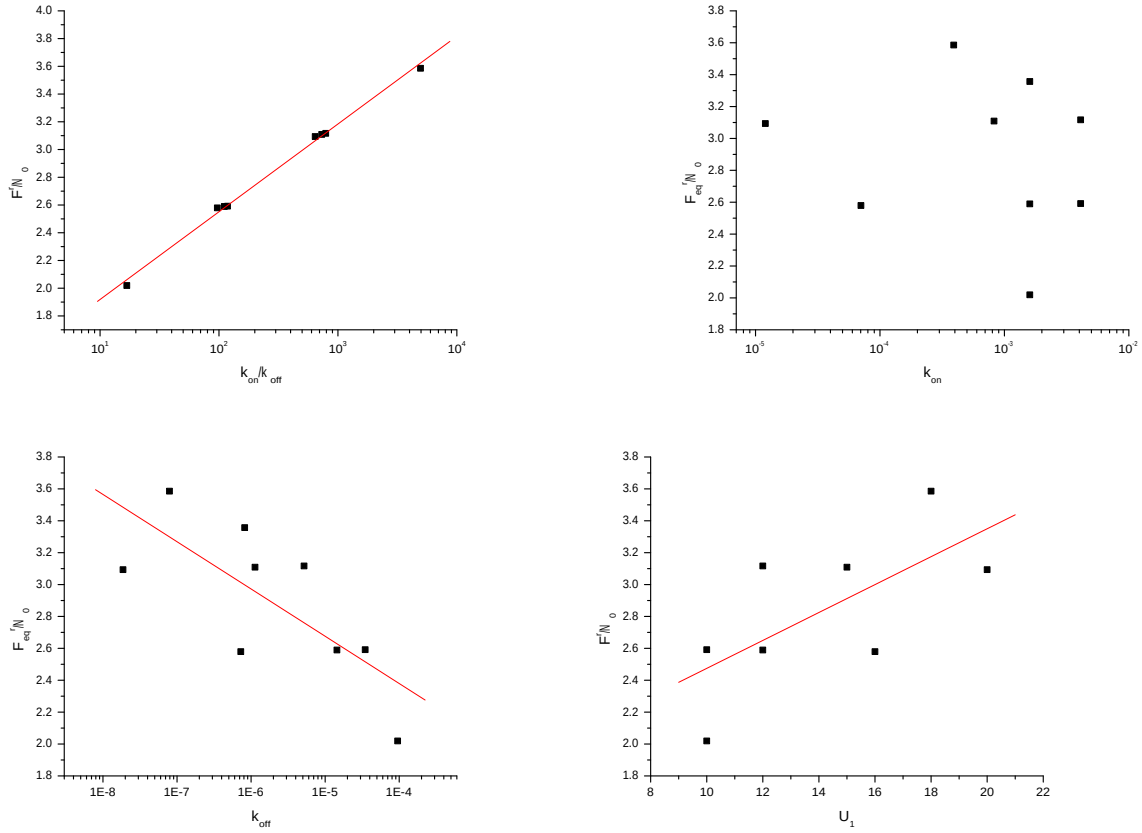

Figure 9: Correlation of the normalized equilibrium rupture force F^r_{eq}/N_0 and thermodynamic parameters in the near-equilibrium regime.

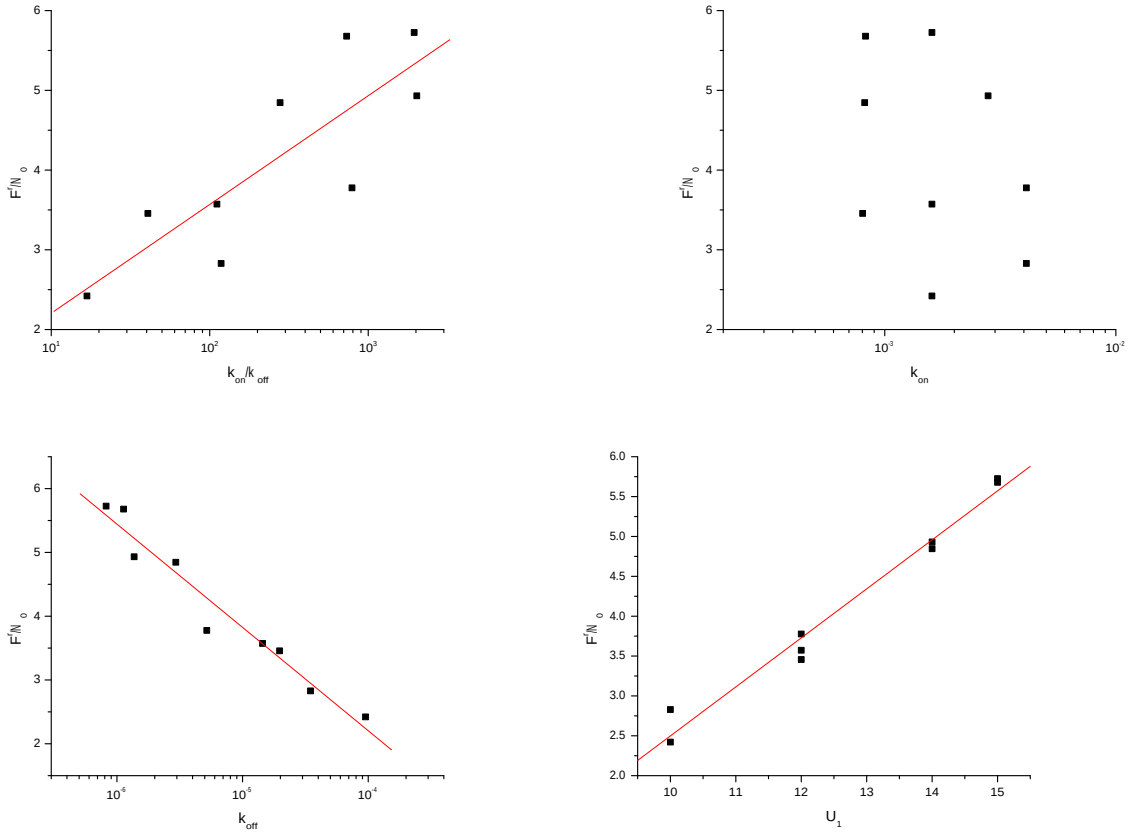

Figure 10: Correlation of the normalized rupture force F^r/N_0 and thermodynamic parameters in the non-equilibrium regime. The rupture force F^r is obtained from the Brownian dynamics simulations.

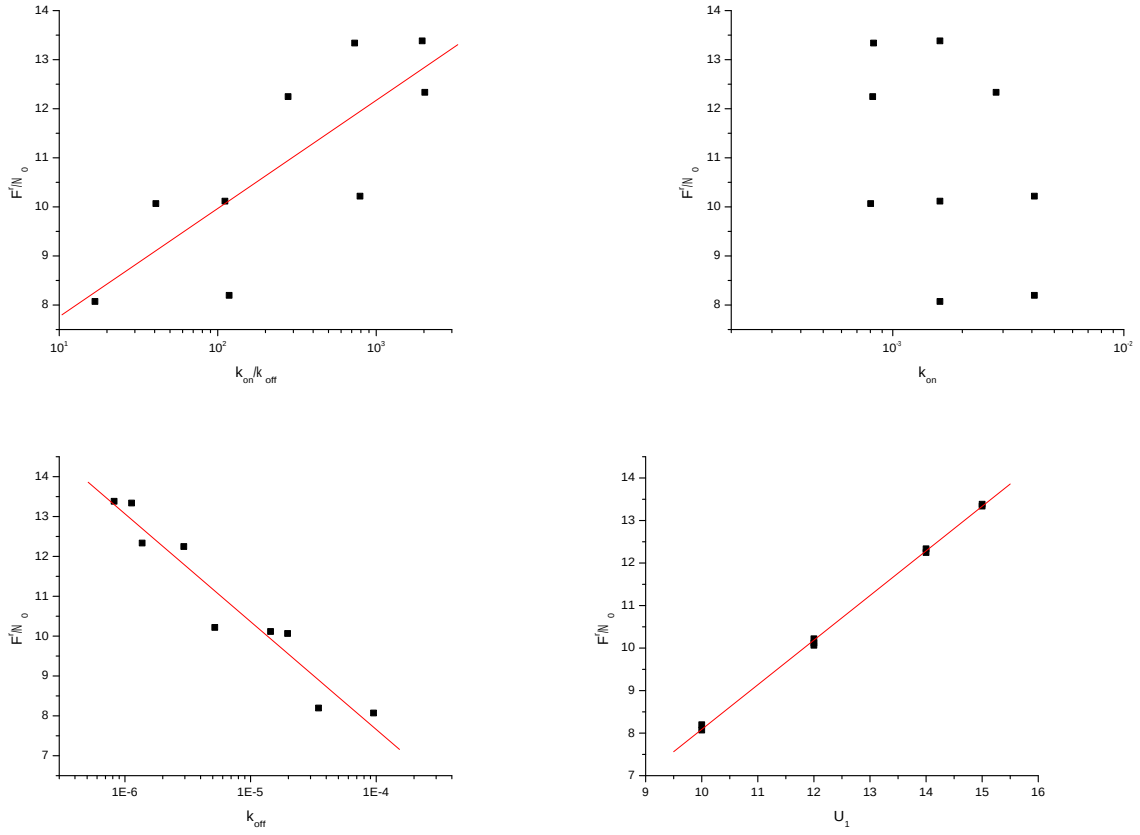

Figure 11: Correlation of the normalized rupture force F^r/N_0 and thermodynamic parameters in the far-from-equilibrium regime. The rupture force F^r is obtained from the Brownian dynamics simulations.

List of Recent TAM Reports

No.	*Authors*	*Title*	*Date*
1005	Fried, E., and B. C. Roy	Gravity-induced segregation of cohesionless granular mixtures—*Lecture Notes in Mechanics*, in press (2002)	July 2002
1006	Tomkins, C. D., and R. J. Adrian	Spanwise structure and scale growth in turbulent boundary layers—*Journal of Fluid Mechanics* (submitted)	Aug. 2002
1007	Riahi, D. N.	On nonlinear convection in mushy layers: Part 2. Mixed oscillatory and stationary modes of convection—*Journal of Fluid Mechanics* **517**, 71–102 (2004)	Sept. 2002
1008	Aref, H., P. K. Newton, M. A. Stremler, T. Tokieda, and D. L. Vainchtein	Vortex crystals—*Advances in Applied Mathematics* **39**, in press (2002)	Oct. 2002
1009	Bagchi, P., and S. Balachandar	Effect of turbulence on the drag and lift of a particle—*Physics of Fluids*, in press (2003)	Oct. 2002
1010	Zhang, S., R. Panat, and K. J. Hsia	Influence of surface morphology on the adhesive strength of aluminum/epoxy interfaces—*Journal of Adhesion Science and Technology* **17**, 1685–1711 (2003)	Oct. 2002
1011	Carlson, D. E., E. Fried, and D. A. Tortorelli	On internal constraints in continuum mechanics—*Journal of Elasticity* **70**, 101–109 (2003)	Oct. 2002
1012	Boyland, P. L., M. A. Stremler, and H. Aref	Topological fluid mechanics of point vortex motions—*Physica D* **175**, 69–95 (2002)	Oct. 2002
1013	Bhattacharjee, P., and D. N. Riahi	Computational studies of the effect of rotation on convection during protein crystallization—*International Journal of Mathematical Sciences* **3**, 429–450 (2004)	Feb. 2003
1014	Brown, E. N., M. R. Kessler, N. R. Sottos, and S. R. White	*In situ* poly(urea-formaldehyde) microencapsulation of dicyclopentadiene—*Journal of Microencapsulation* (submitted)	Feb. 2003
1015	Brown, E. N., S. R. White, and N. R. Sottos	Microcapsule induced toughening in a self-healing polymer composite—*Journal of Materials Science* (submitted)	Feb. 2003
1016	Kuznetsov, I. R., and D. S. Stewart	Burning rate of energetic materials with thermal expansion—*Combustion and Flame* (submitted)	Mar. 2003
1017	Dolbow, J., E. Fried, and H. Ji	Chemically induced swelling of hydrogels—*Journal of the Mechanics and Physics of Solids*, in press (2003)	Mar. 2003
1018	Costello, G. A.	Mechanics of wire rope—Mordica Lecture, Interwire 2003, Wire Association International, Atlanta, Georgia, May 12, 2003	Mar. 2003
1019	Wang, J., N. R. Sottos, and R. L. Weaver	Thin film adhesion measurement by laser induced stress waves—*Journal of the Mechanics and Physics of Solids* (submitted)	Apr. 2003
1020	Bhattacharjee, P., and D. N. Riahi	Effect of rotation on surface tension driven flow during protein crystallization—*Microgravity Science and Technology* **14**, 36–44 (2003)	Apr. 2003
1021	Fried, E.	The configurational and standard force balances are not always statements of a single law—*Proceedings of the Royal Society* (submitted)	Apr. 2003
1022	Panat, R. P., and K. J. Hsia	Experimental investigation of the bond coat rumpling instability under isothermal and cyclic thermal histories in thermal barrier systems—*Proceedings of the Royal Society of London A* **460**, 1957–1979 (2003)	May 2003
1023	Fried, E., and M. E. Gurtin	A unified treatment of evolving interfaces accounting for small deformations and atomic transport: grain-boundaries, phase transitions, epitaxy—*Advances in Applied Mechanics* **40**, 1–177 (2004)	May 2003
1024	Dong, F., D. N. Riahi, and A. T. Hsui	On similarity waves in compacting media—*Horizons in World Physics* **244**, 45–82 (2004)	May 2003
1025	Liu, M., and K. J. Hsia	Locking of electric field induced non-180° domain switching and phase transition in ferroelectric materials upon cyclic electric fatigue—*Applied Physics Letters* **83**, 3978–3980 (2003)	May 2003

List of Recent TAM Reports (cont'd)

No.	*Authors*	*Title*	*Date*
1026	Liu, M., K. J. Hsia, and M. Sardela Jr.	In situ X-ray diffraction study of electric field induced domain switching and phase transition in PZT-5H—*Journal of the American Ceramics Society* (submitted)	May 2003
1027	Riahi, D. N.	On flow of binary alloys during crystal growth—*Recent Research Development in Crystal Growth* **3**, 49–59 (2003)	May 2003
1028	Riahi, D. N.	On fluid dynamics during crystallization—*Recent Research Development in Fluid Dynamics* **4**, 87–94 (2003)	July 2003
1029	Fried, E., V. Korchagin, and R. E. Todres	Biaxial disclinated states in nematic elastomers—*Journal of Chemical Physics* **119**, 13170–13179 (2003)	July 2003
1030	Sharp, K. V., and R. J. Adrian	Transition from laminar to turbulent flow in liquid filled microtubes—*Physics of Fluids* (submitted)	July 2003
1031	Yoon, H. S., D. F. Hill, S. Balachandar, R. J. Adrian, and M. Y. Ha	Reynolds number scaling of flow in a Rushton turbine stirred tank: Part I—Mean flow, circular jet and tip vortex scaling—*Chemical Engineering Science* (submitted)	Aug. 2003
1032	Raju, R., S. Balachandar, D. F. Hill, and R. J. Adrian	Reynolds number scaling of flow in a Rushton turbine stirred tank: Part II—Eigen-decomposition of fluctuation—*Chemical Engineering Science* (submitted)	Aug. 2003
1033	Hill, K. M., G. Gioia, and V. V. Tota	Structure and kinematics in dense free-surface granular flow—*Physical Review Letters* **91**, 064302 (2003)	Aug. 2003
1034	Fried, E., and S. Sellers	Free-energy density functions for nematic elastomers—*Journal of the Mechanics and Physics of Solids* **52**, 1671–1689 (2004)	Sept. 2003
1035	Kasimov, A. R., and D. S. Stewart	On the dynamics of self-sustained one-dimensional detonations: A numerical study in the shock-attached frame—*Physics of Fluids* (submitted)	Nov. 2003
1036	Fried, E., and B. C. Roy	Disclinations in a homogeneously deformed nematic elastomer—*Nature Materials* (submitted)	Nov. 2003
1037	Fried, E., and M. E. Gurtin	The unifying nature of the configurational force balance—*Mechanics of Material Forces* (P. Steinmann and G. A. Maugin, eds.), in press (2003)	Dec. 2003
1038	Panat, R., K. J. Hsia, and J. W. Oldham	Rumpling instability in thermal barrier systems under isothermal conditions in vacuum—*Philosophical Magazine*, in press (2004)	Dec. 2003
1039	Cermelli, P., E. Fried, and M. E. Gurtin	Sharp-interface nematic–isotropic phase transitions without flow—*Archive for Rational Mechanics and Analysis* **174**, 151–178 (2004)	Dec. 2003
1040	Yoo, S., and D. S. Stewart	A hybrid level-set method in two and three dimensions for modeling detonation and combustion problems in complex geometries—*Combustion Theory and Modeling* (submitted)	Feb. 2004
1041	Dienberg, C. E., S. E. Ott-Monsivais, J. L. Ranchero, A. A. Rzeszutko, and C. L. Winter	Proceedings of the Fifth Annual Research Conference in Mechanics (April 2003), TAM Department, UIUC (E. N. Brown, ed.)	Feb. 2004
1042	Kasimov, A. R., and D. S. Stewart	Asymptotic theory of ignition and failure of self-sustained detonations—*Journal of Fluid Mechanics* (submitted)	Feb. 2004
1043	Kasimov, A. R., and D. S. Stewart	Theory of direct initiation of gaseous detonations and comparison with experiment—*Proceedings of the Combustion Institute* (submitted)	Mar. 2004
1044	Panat, R., K. J. Hsia, and D. G. Cahill	Evolution of surface waviness in thin films via volume and surface diffusion—*Journal of Applied Physics* (submitted)	Mar. 2004
1045	Riahi, D. N.	Steady and oscillatory flow in a mushy layer—*Current Topics in Crystal Growth Research*, in press (2004)	Mar. 2004
1046	Riahi, D. N.	Modeling flows in protein crystal growth—*Current Topics in Crystal Growth Research*, in press (2004)	Mar. 2004
1047	Bagchi, P., and S. Balachandar	Response of the wake of an isolated particle to isotropic turbulent cross-flow—*Journal of Fluid Mechanics* (submitted)	Mar. 2004

List of Recent TAM Reports (cont'd)

No.	*Authors*	*Title*	*Date*
1048	Brown, E. N., S. R. White, and N. R. Sottos	Fatigue crack propagation in microcapsule toughened epoxy—*Journal of Materials Science* (submitted)	Apr. 2004
1049	Zeng, L., S. Balachandar, and P. Fischer	Wall-induced forces on a rigid sphere at finite Reynolds number—*Journal of Fluid Mechanics* (submitted)	May 2004
1050	Dolbow, J., E. Fried, and H. Ji	A numerical strategy for investigating the kinetic response of stimulus-responsive hydrogels—*Computer Methods in Applied Mechanics and Engineering* **194**, 4447–4480 (2005)	June 2004
1051	Riahi, D. N.	Effect of permeability on steady flow in a dendrite layer—*Journal of Porous Media*, in press (2004)	July 2004
1052	Cermelli, P., E. Fried, and M. E. Gurtin	Transport relations for surface integrals arising in the formulation of balance laws for evolving fluid interfaces—*Journal of Fluid Mechanics* (submitted)	Sept. 2004
1053	Stewart, D. S., and A. R. Kasimov	Theory of detonation with an embedded sonic locus—*SIAM Journal on Applied Mathematics* (submitted)	Oct. 2004
1054	Stewart, D. S., K. C. Tang, S. Yoo, M. Q. Brewster, and I. R. Kuznetsov	Multi-scale modeling of solid rocket motors: Time integration methods from computational aerodynamics applied to stable quasi-steady motor burning—*Proceedings of the 43rd AIAA Aerospace Sciences Meeting and Exhibit* (January 2005), Paper AIAA-2005-0357 (2005)	Oct. 2004
1055	Ji, H., H. Mourad, E. Fried, and J. Dolbow	Kinetics of thermally induced swelling of hydrogels—*International Journal of Solids and Structures* (submitted)	Dec. 2004
1056	Fulton, J. M., S. Hussain, J. H. Lai, M. E. Ly, S. A. McGough, G. M. Miller, R. Oats, L. A. Shipton, P. K. Shreeman, D. S. Widrevitz, and E. A. Zimmermann	Final reports: Mechanics of complex materials, Summer 2004 (K. M. Hill and J. W. Phillips, eds.)	Dec. 2004
1057	Hill, K. M., G. Gioia, and D. R. Amaravadi	Radial segregation patterns in rotating granular mixtures: Waviness selection—*Physical Review Letters* **93**, 224301 (2004)	Dec. 2004
1058	Riahi, D. N.	Nonlinear oscillatory convection in rotating mushy layers—*Journal of Fluid Mechanics*, in press (2005)	Dec. 2004
1059	Okhuysen, B. S., and D. N. Riahi	On buoyant convection in binary solidification—*Journal of Fluid Mechanics* (submitted)	Jan. 2005
1060	Brown, E. N., S. R. White, and N. R. Sottos	Retardation and repair of fatigue cracks in a microcapsule toughened epoxy composite—Part I: Manual infiltration—*Composites Science and Technology* (submitted)	Jan. 2005
1061	Brown, E. N., S. R. White, and N. R. Sottos	Retardation and repair of fatigue cracks in a microcapsule toughened epoxy composite—Part II: *In situ* self-healing—*Composites Science and Technology* (submitted)	Jan. 2005
1062	Berfield, T. A., R. J. Ong, D. A. Payne, and N. R. Sottos	Residual stress effects on piezoelectric response of sol-gel derived PZT thin films—*Journal of Applied Physics* (submitted)	Apr. 2005
1063	Anderson, D. M., P. Cermelli, E. Fried, M. E. Gurtin, and G. B. McFadden	General dynamical sharp-interface conditions for phase transformations in viscous heat-conducting fluids—*Journal of Fluid Mechanics* (submitted)	Apr. 2005
1064	Fried, E., and M. E. Gurtin	Second-gradient fluids: A theory for incompressible flows at small length scales—*Journal of Fluid Mechanics* (submitted)	Apr. 2005
1065	Gioia, G., and F. A. Bombardelli	Localized turbulent flows on scouring granular beds—*Physical Review Letters*, in press (2005)	May 2005
1066	Fried, E., and S. Sellers	Orientational order and finite strain in nematic elastomers—*Journal of Chemical Physics* **123**, 044901 (2005)	May 2005

List of Recent TAM Reports (cont'd)

No.	*Authors*	*Title*	*Date*
1067	Chen, Y.-C., and E. Fried	Uniaxial nematic elastomers: Constitutive framework and a simple application—*Proceedings of the Royal Society of London A*, in press (2005)	June 2005
1068	Fried, E., and S. Sellers	Incompatible strains associated with defects in nematic elastomers—*Journal of Chemical Physics*, in press (2005)	Aug. 2005
1069	Gioia, G., and X. Dai	Surface stress and reversing size effect in the initial yielding of ultrathin films—*Journal of Applied Mechanics*, in press (2005)	Aug. 2005
1070	Gioia, G., and P. Chakraborty	Turbulent friction in rough pipes and the energy spectrum of the phenomenological theory—*Physical Review Letters* **96**, 044502 (2006)	Aug. 2005
1071	Keller, M. W., and N. R. Sottos	Mechanical properties of capsules used in a self-healing polymer—*Experimental Mechanics* (submitted)	Sept. 2005
1072	Chakraborty, P., G. Gioia, and S. Kieffer	Volcán Reventador's unusual umbrella	Sept. 2005
1073	Fried, E., and S. Sellers	Soft elasticity is not necessary for striping in nematic elastomers—*Nature Physics* (submitted)	Sept. 2005
1074	Fried, E., M. E. Gurtin, and Amy Q. Shen	Theory for solvent, momentum, and energy transfer between a surfactant solution and a vapor atmosphere—*Physical Review E* (submitted)	Sept. 2005
1075	Chen, X., and E. Fried	Rayleigh–Taylor problem for a liquid–liquid phase interface—*Journal of Fluid Mechanics* (submitted)	Oct. 2005
1076	Riahi, D. N.	Mathematical modeling of wind forces—In *The Euler Volume* (Abington, UK: Taylor and Francis), in press (2005)	Oct. 2005
1077	Fried, E., and R. E. Todres	Mind the gap: The shape of the free surface of a rubber-like material in the proximity to a rigid contactor—*Journal of Elasticity*, in press (2006)	Oct. 2005
1078	Riahi, D. N.	Nonlinear compositional convection in mushy layers—*Journal of Fluid Mechanics* (submitted)	Dec. 2005
1079	Bhattacharjee, P., and D. N. Riahi	Mathematical modeling of flow control using magnetic fluid and field—In *The Euler Volume* (Abington, UK: Taylor and Francis), in press (2005)	Dec. 2005
1080	Bhattacharjee, P., and D. N. Riahi	A hybrid level set/VOF method for the simulation of thermal magnetic fluids—*International Journal for Numerical Methods in Engineering* (submitted)	Dec. 2005
1081	Bhattacharjee, P., and D. N. Riahi	Numerical study of surface tension driven convection in thermal magnetic fluids—*Journal of Crystal Growth* (submitted)	Dec. 2005
1082	Riahi, D. N.	Inertial and Coriolis effects on oscillatory flow in a horizontal dendrite layer—*Transport in Porous Media* (submitted)	Jan. 2006
1083	Wu, Y., and K. T. Christensen	Population trends of spanwise vortices in wall turbulence—*Journal of Fluid Mechanics* (submitted)	Jan. 2006
1084	Natrajan, V. K., and K. T. Christensen	The role of coherent structures in subgrid-scale energy transfer within the log layer of wall turbulence—*Physics of Fluids* (submitted)	Jan. 2006
1085	Wu, Y., and K. T. Christensen	Reynolds-stress enhancement associated with a short fetch of roughness in wall turbulence—*AIAA Journal* (submitted)	Jan. 2006
1086	Fried, E., and M. E. Gurtin	Cosserat fluids and the continuum mechanics of turbulence: A generalized Navier–Stokes-α equation with complete boundary conditions—*Journal of Fluid Mechanics* (submitted)	Feb. 2006
1087	Riahi, D. N.	Inertial effects on rotating flow in a porous layer—*Journal of Porous Media* (submitted)	Feb. 2006
1088	Li, F., and D. E. Leckband	Dynamic strength of adhesion surfaces—*Journal of Chemical Physics* (submitted)	Mar. 2006